Journal of Physics: Conference Series **198** (2009) 012005 doi:10.1088/1742-6596/198/1/012005

Compton scattering at high intensities

Thomas Heinzl

University of Plymouth, School of Mathematics and Statistics, Drake Circus, Plymouth PL4 8AA, UK

E-mail: thomas.heinzl@plymouth.ac.uk

Abstract. High-intensity Compton scattering takes place when an electron beam is brought into collision with a high power laser. We briefly review the main intensity signatures using the formalism of strong-field quantum electrodynamics.

1. Introduction

Strong field quantum electrodynamics (QED) arises as a slight modification of ordinary QED upon adding a strong *external* electromagnetic field. Traditionally, this would have been the static Coulomb field of a nucleus or a heavy ion leading to effects such as Bremsstrahlung, pair creation [1] or Delbrück scattering [2]. In recent years, huge, time-dependent electromagnetic fields have been produced using high-power lasers, and this will be the focus of this presentation. The magnitudes of some characteristic physical quantities assumed for the purposes of this talk are given in Table 1.

Table 1. Some typical magnitudes characterising current high-power lasers.

Quantity	Magnitude
Power	$P \gtrsim 10^{15}\,\mathrm{W} = 1\,\mathrm{PW}$
Intensity	$I \gtrsim 10^{22}\,\mathrm{W/cm^2}$
Electric field	$E \gtrsim 10^{14}\,\mathrm{V/m}$
Magnetic field	$B \gtrsim 10^{10}\,\mathrm{G} = 10^{6}\,\mathrm{T}$

Within the next few years one expects to achieve intensities of 10^{23} W/cm^2 at the Vulcan 10 PW upgrade facility [3] and possibly 10^{26} W/cm^2 once the European Extreme Light Infrastructure (ELI) is realised [4]. The currently achieved field strengths should be compared with the genuine QED electric field first obtained by Sauter [5],

$$E_{\mathrm{S}} = \frac{m^2}{e} = 1.3 \times 10^{18}\,\mathrm{V/m}\,, \tag{1}$$

where m is the electron mass and e its charge. The field strength (1) implies an intensity of about 10^{30} W/cm^2. For such extreme magnitudes it becomes energetically favourable for the

vacuum to 'break down' by producing electron positron pairs in order to screen and hence lower the external field (see e.g. [6] for a lucid discussion). The process involved may be interpreted as a nonperturbative tunneling phenomenon and hence is exponentially suppressed [7, 8, 9]. Although there is a huge kinematic pre-exponential factor which somewhat compensates the exponential suppression, current estimates do not predict these 'Schwinger' pairs below 10^{27} W/cm^2. Technically, pair production is signalled by the appearance of an imaginary part in the expression for vacuum polarisation (dressed by the strong external field). The real part, however, is interesting as well as it describes the propagation of photons modified by vacuum polarisation effects, which become magnified and directional due to the external fields present. Possibly most striking is the effect of 'vacuum birefringence', i.e. the occurrence of a phase retardation due to two different and nontrivial refractive indices for different polarisation directions. This was first discussed in Toll's unpublished thesis [10] (see also [11, 12]) and was recently reinvestigated in the light of new laser developments [13] (see also [14]). To enhance the birefringence signal, the strong fields should be probed by an X-ray beam. With current X-ray polarimetry techniques one requires an intensity of at least 10^{25} W/cm^2 to achieve measurable magnitude for the phase retardation effect.

The upshot of this discussion is that strong field vacuum polarisation effects remain elusively small until one gets sufficiently close to the critical field strength (1). Alternatively, one may leave the regime of low energy and use probes (photons or electrons) with energies comparable to the electron mass m or larger. There is, however, a strong field process where intensity effects may readily be studied at low energies and current intensities as given in Table 1. This is high-intensity (or nonlinear) Compton scattering to which we now turn our attention, reviewing our recent analysis [15].

2. Nonlinear Compton scattering: Overview

Our goal is to identify and isolate intensity effects on the spectrum of photons emitted in collisions of a high-power laser with an electron beam. To this end it is useful to define a dimensionless measure of laser intensity via

$$a_0 \equiv \frac{eE\lambda\!\!\!^{-}}{m} = \frac{eE}{\omega m} \,, \tag{2}$$

where E is the r.m.s. electric field of the laser having wavelength λ ($\lambda\!\!\!^{-} \equiv \lambda/2\pi = 1/\omega$). Note that a_0 is a purely classical ratio measuring the energy gain of an electron travelling a distance $\lambda\!\!\!^{-}$ in the laser field in units of its rest energy, m. Thus, intensity is determined by means of a *probe*, chosen to be an electron. Once a_0 exceeds unity the quiver motion of the probe electron within the beam becomes relativistic. From a particle physics perspective the definition (2) appears gauge invariant as it only involves the field strength, but Lorentz invariance seems lost. The latter may be recovered by writing $a_0^2 = -e^2\mathsf{A}^2/m^2$ [16, 17] with $\mathsf{A}^2 = \mathsf{A}_\mu\mathsf{A}^\mu$ being the squared gauge potential (suitably time averaged), but this obviously sacrifices gauge invariance. The way out is provided by the Lorentz and gauge invariant definition [18]

$$a_0^2 \equiv \frac{e^2}{m^2}\frac{\langle p_\mu T^{\mu\nu} p_\nu\rangle}{(k\cdot p)^2} \,, \tag{3}$$

in terms of the electron and photon four-momenta, p and k, and the Maxwell energy momentum tensor, $T^{\mu\nu}$. The brackets $\langle\,.\,\rangle$ denote a Lorentz invariant average over proper time. Note that in the electron rest frame where $p = (m, \mathbf{0})$ we indeed reproduce (2) using $T^{00} = E^2$. We conclude these preliminary remarks, by providing an overview of current and planned laser facilities and their associated intensities in Table 2.

Table 2. Absolute and normalised intensities of current and planned laser facilities. (XFEL: X-ray free electron laser at DESY, Hamburg, FZD: Forschungszentrum Dresden-Rossendorf, Vulcan at Central Laser Facility, Rutherford laboratory [3], ELI: Extreme Light Infrastructure project [4], HiPER: High Power laser Energy Research facility project [19])

	XFEL ('goal')	FZD Draco	Vulcan (1 PW)	Vulcan (10 PW)	ELI/HiPER
I [W/cm^2]	10^{27}	10^{21}	10^{22}	10^{23}	10^{26}
a_0	10	20	70	200	5×10^3

Note that $a_0 \gg 1$ is characteristic for *optical* lasers as the larger frequency of an XFEL reduces the a_0 value according to (2). Thus, henceforth we will assume a scenario where an electron beam collides with photons from an optical laser. To further simplify our analysis we consider a head-on collision only, as schematically sketched in Fig. 1. Before reviewing the strong-field

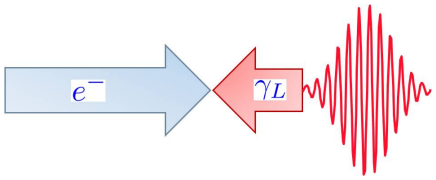

Figure 1. Schematic scenario for nonlinear Compton scattering: an electron beam (e^-) is brought into collision with a laser (γ_L). We concentrate on the special case of a head-on collision.

QED analysis of such a process let us briefly discuss the main intensity effects classically. In principle one can solve for the classical trajectory of the electron subjected to the beam (taken to be a circularly polarised plane wave) and plug the result into the classical formula for the intensity distribution of the ensuing radiation [20]. As the orbits in question are circular one recovers the spectrum first obtained by Schott almost a century ago [21] (see also [22]). The basic intensity effect may already be seen from the first integral of the equation of motion, $p^\mu(\tau)$. Taking the proper time average one finds a mean or quasi momentum given by

$$q^\mu \equiv \langle p^\mu(\tau) \rangle = p^\mu + \frac{a_0^2\, m^2}{2\, k\cdot p}\, k^\mu \equiv p^\mu + q_L^\mu \,, \tag{4}$$

which explicitly depends on the intensity parameter a_0 and squares to an effective electron mass

$$q^2 \equiv m_*^2 = m^2(1 + a_0^2) \,, \tag{5}$$

as first obtained by Sengupta [23, 24] and thoroughly discussed in [25]. The zero component of (4), i.e. the average energy shift, was found previously by Volkov upon solving the Dirac equation in a plane wave [26] described by a gauge potential $\mathsf{A}_\mu = \mathsf{A}_\mu(\xi)$, $\xi = k\cdot x$, with k being the four-momentum of the wave. The Volkov solution is then given by the four-spinor,

$$\Psi_{\boldsymbol{p}}(x) = \exp\left\{ -ip\cdot x + \frac{1}{2ik\cdot p}\int^{k\cdot x} d\xi \left(2ep\cdot \mathsf{A}(\xi) - e^2\mathsf{A}^2(\xi) \right) \right\} \chi_{\boldsymbol{p}} \,, \tag{6}$$

where $\chi_{\boldsymbol{p}}$ is a combination of Dirac matrices acting on the standard free Dirac spinor u, see e.g. [15, 17]. The exponent is the classical Hamilton-Jacobi action for an electron in a plane

wave. Assuming circular polarisation, $\mathsf{A}^\mu = a_1^\mu \cos(k\cdot x) + a_2^\mu \sin(k\cdot x)$, with $k^2 = 0 = a_i \cdot k$ and $a_i \cdot a_j = -a^2\delta_{ij}$, the Volkov solution (6) becomes

$$\Psi_{\boldsymbol{p}}(x) = \exp\left\{ -iq\cdot x - ie\frac{a_1\cdot p}{k\cdot p}\,\sin(k\cdot x) + ie\frac{a_2\cdot p}{k\cdot p}\,\cos(k\cdot x)\right\}\chi_{\boldsymbol{p}}\,. \tag{7}$$

We see the quasi-momentum q making its appearance in the exponent, its longitudinal part q_L stemming from the zero momentum mode of A^2 in (6), $q_L \sim \langle \mathsf{A}^2\rangle \sim a_0^2$.

The Volkov solution (6) is a crucial ingredient for the formalism of strong-field QED in plane wave backgrounds A based on what is called the Furry picture [27]. Basically, this amounts to altering the decomposition of the Hamiltonian into free and interacting parts by including the background field into the former. In this way, the background is treated exactly while the fluctuations around it are taken into account perturbatively. In this vein, one replaces standard ('bare') fermion lines in Feynman diagrams by *dressed* ones. For external lines, free Dirac wave functions like e.g. $ue^{ip\cdot x}$ are replaced by Volkov wave functions, (6) or (7). Pictorially, this is shown in Fig. 2.

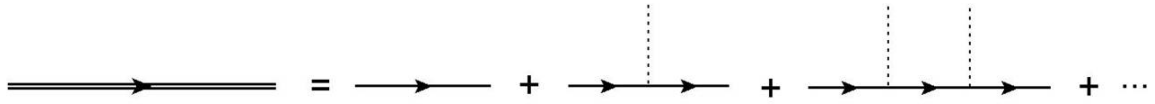

Figure 2. Dressed fermion line expanded in terms of bare ones. The external plane wave field is given by the dotted lines representing continuous absorption/emission of laser photons.

Let us now specialise to nonlinear Compton scattering where a photon γ is emitted upon collisions of electron and laser beams. The Furry picture diagram may be expanded into a series of subprocesses where n laser photons γ_L are being absorbed,

$$e + n\gamma_L = e' + \gamma\,, \tag{8}$$

as shown in Fig. 3.

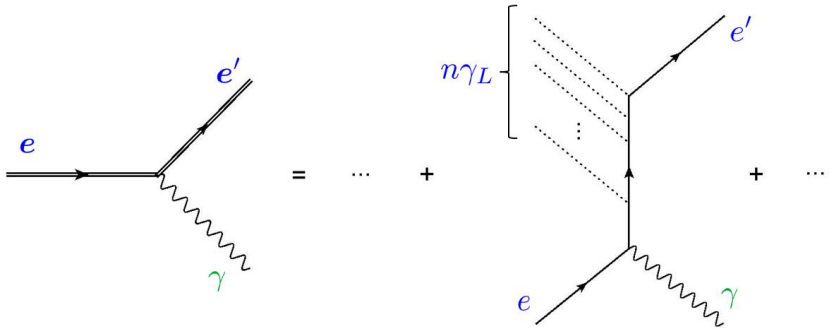

Figure 3. Feynman diagrams for nonlinear Compton scattering. The Furry picture diagram on the left (with dressed electrons) is expanded into an infinite series of subprocesses, $e + n\gamma_L = e' + \gamma$.

The left-hand side of Fig. 3 represents the Furry picture S-matrix element [28, 29, 30]

$$S_{fi} \sim -ie\int \bar\Psi_{\boldsymbol{p}'}\not{\mathsf{A}}\Psi_{\boldsymbol{p}}\,, \tag{9}$$

which indeed is built from external Volkov lines (so is exact in the background), but otherwise is first order in the fluctuation field A representing the emitted photon γ. Evaluating this expression one recovers the diagrams on the right-hand side of Fig. 3, however, with a nonstandard momentum assignment. The electrons carry quasi-momenta q and q' rather than the asymptotic momenta p and p' in the absence of the field. Accordingly, momentum conservation for each sub-process reads

$$q + nk = q' + k' \,, \tag{10}$$

with k and k' denoting the momenta of laser and emitted photons, respectively. The processes (8) have been observed before in the experiment SLAC E-144 [31] where a Terawatt laser beam was brought into collision with the 50 GeV electron beam provided by SLAC. As a result the emitted photons had a rather high energy of about 30 GeV. However, only the energy spectra of the outgoing electrons have been recorded and were found to be in agreement with the theory employing the Furry picture (9) as summarised in [16]. The emission rates and spectral distributions of the outgoing photons have not been measured yet but there are plans to do so in the near future at Daresbury laboratories and FZD. Both facilities are working at comparatively low energies, with electron beams in the few 10 MeV range and intensities implying a_0 values of order 10. It is important to note that this regime of strong-field QED (low energies, large intensities) has not been tested before. The expected outcome of these experiments is the topic of the next section.

3. Nonlinear Compton scattering: Results

Before discussing photon emission rates and spectra a few words on the kinematics are in order. Let us first recall the Compton formula for the scattered frequency in the lab frame,

$$\omega' = \frac{\omega}{1 + (\omega/m - \sinh\zeta)\, e^{-\zeta}\,(1 - \cos\theta)} \,, \tag{11}$$

where the electrons are characterised by rapidity ζ via $e^{\zeta} = \gamma(1+\beta)$ (β and γ being the usual Lorentz factors) and θ is the usual scattering angle (between $\boldsymbol{k}$ and $\boldsymbol{k}'$). When we generalise this to the nonlinear processes (8) the intensity dependence of the quasi-momenta in (10) is inherited by the scattered frequency such that (11) is superseded by

$$\omega' = \frac{n\,\omega}{1 + \kappa_n\, e^{-\zeta}\,(1 - \cos\theta)} \,. \tag{12}$$

Here we have defined the dimensionless projection of the total momentum $\boldsymbol{P} \equiv \boldsymbol{q} + n\boldsymbol{k}$ onto the direction $\hat{\boldsymbol{k}}$,

$$\kappa_n = -\boldsymbol{P}\cdot\hat{\boldsymbol{k}}/m = n\omega/m - \sinh\zeta + a_0^2 e^{-\zeta/2} \,. \tag{13}$$

Comparing with ordinary Compton scattering (11) we see that (i) the laser frequency ω is replaced by $n\omega$ and (ii) there is a new, intensity dependent addition signalled by the presence of a_0. Item (i) is often referred to as 'higher harmonics generation' and has indeed been observed before by studying the azimuthal intensity distribution of radiation using *linearly* polarised laser light. Second and third harmonics could be identified via their typical quadrupole and sextupole patterns [32, 33].

The main effect, however, to be inferred from (12) is a shift of the Compton edge. To see what is involved let us first consider linear Compton scattering (11). For sufficiently large electron energies ($p^0 \gg m$ or $\gamma \gg 1$) the maximum frequency is obtained for backscattering ($\theta = \pi$), namely

$$\omega'_{\max} \simeq 4\gamma^2\omega \,, \tag{14}$$

which corresponds to a *blue-shift* compared to the incoming laser frequency, $\omega' > \omega$. This is often referred to as 'inverse Compton scattering': in the lab frame the electrons transfer energy to the photons[1]. In the nonlinear case, for the same kinematic situation and $a_0 \gg 1$, the edge value (14) is replaced by the intensity dependent answer,

$$\omega'_{n,\max} \simeq 4\gamma^2 n\omega/a_0^2 \,. \tag{15}$$

Thus, while there is still an overall blue-shift (as long as $a_0 \lesssim 2\gamma$) the result (15) implies an intensity dependent red-shift of the $n = 1$ Compton edge (14) according to

$$\omega'_{\max} \simeq 4\gamma^2\omega \to 4\gamma^2\omega/a_0^2 \,. \tag{16}$$

Intuitively this may be explained as follows. Because of its larger effective mass, $m_* > m$, the electron is more static and recoils less so that the energy transfer to the photons is reduced. Thus, already at this stage we can see that increasing intensity produces a tendency to go from inverse to ordinary Compton scattering. This frame dependent effect will be quantified in more detail below. Before that, however, let us have a Lorentz invariant look at the photon emission spectra. To this end we define the invariant parameter

$$x \equiv \frac{k\cdot k'}{k\cdot p'} = \frac{n\nu - \nu'}{\kappa_0 + \nu'} \,, \tag{17}$$

where the second identity holds for a head-on collision in the lab frame with $\nu \equiv \omega/m$ and $\nu' \equiv \omega'/m$. Hence, for the parameter regime we are interested in x is basically proportional to scattered frequency [15]. Fig. 4 shows the resulting spectra as function of x for different intensities a_0. One can clearly see the red-shift (16) of the Compton edge compared to the linear Compton edge ($n = 1$, $a_0 = 0$). With increasing a_0 the edge moves further and further to the left to smaller and smaller x i.e. frequency ω'. In addition, there are side maxima to the right of the $n = 1$ edges, signalling the appearance of higher harmonics with $n > 1$.

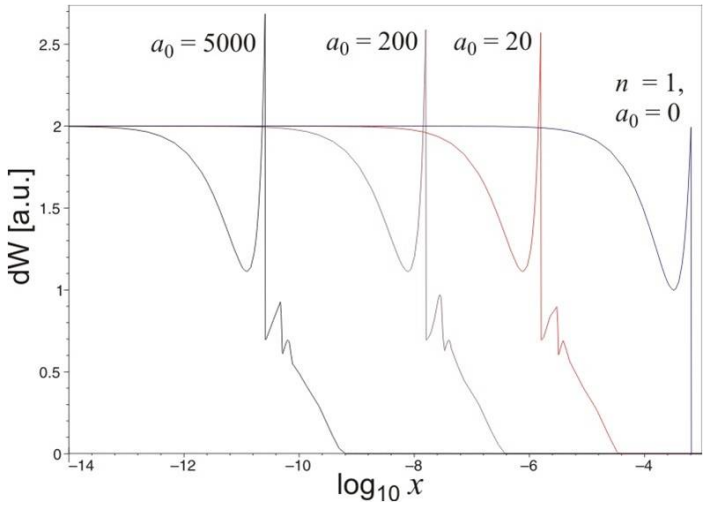

Figure 4. Nonlinear Compton spectra as functions of the invariant x for different values of a_0 and electron energy 40 MeV ($\gamma = 80$, $\nu = \omega/m = 2 \times 10^{-6}$).

If we move on to discussing spectra as a function of scattered frequency ν' there appears a rather rich structure as we tune intensity a_0, displayed in Fig. 5.

[1] Recall that Compton in his original experiment had observed a red-shift upon scattering X-rays off electrons at rest [34].

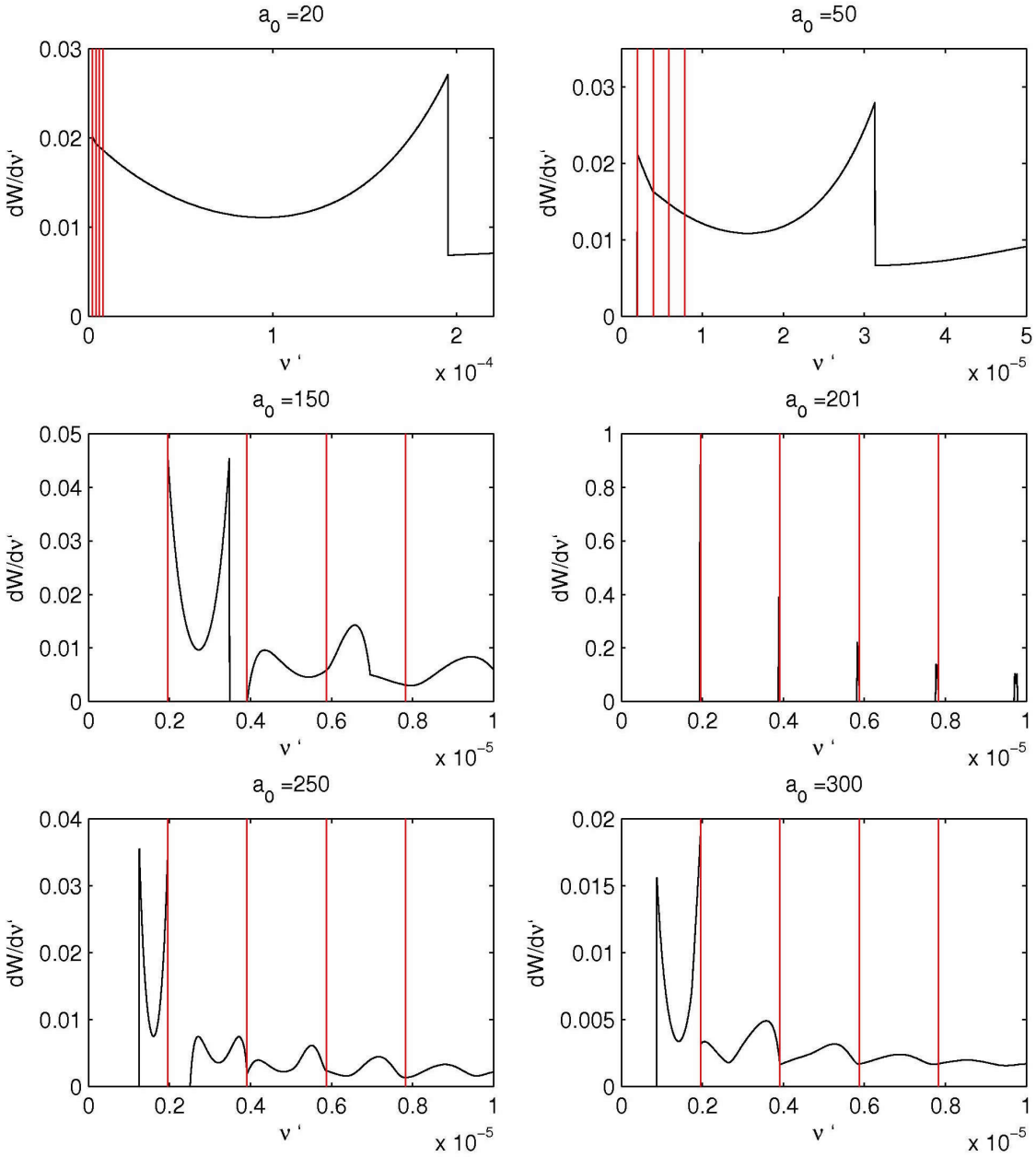

Figure 5. Dependence of the energy spectrum on a_0. The equidistant vertical (red) lines correspond to harmonic frequencies $\nu'_n = n\nu$ (parameters: $\gamma = 100$, $\nu = 2 \times 10^{-6}$).

The spectrum changes significantly upon increasing a_0. For low a_0 values the individual harmonic spectra are all blue-shifted, $\nu'_n > n\nu$, i.e. located to the right of the vertical (red) lines. At $a_0 = 150$ we see a gap appearing between the first and second harmonic and at a critical value, $a_0 \simeq 2\gamma$, the spectrum collapses to (almost) a line spectrum peaked at $\nu'_n = n\nu$, at least for the low harmonics displayed (fourth panel of Fig. 5). Increasing a_0 further the previous blue-

shifts turn into red-shifts, $\nu'_n < n\nu$. In other words, inverse Compton scattering changes into Compton scattering with the boundary being given by the appearance of a line spectrum with fixed values for the scattered frequency, $\nu'_n = n\nu$. One may say that this defines an intensity dependent centre-of-mass system where $a_0 \simeq 2\gamma$. This is further elucidated in Fig. 6 which shows the relation between the relevant three-momenta associated with the spectra of Fig. 5.

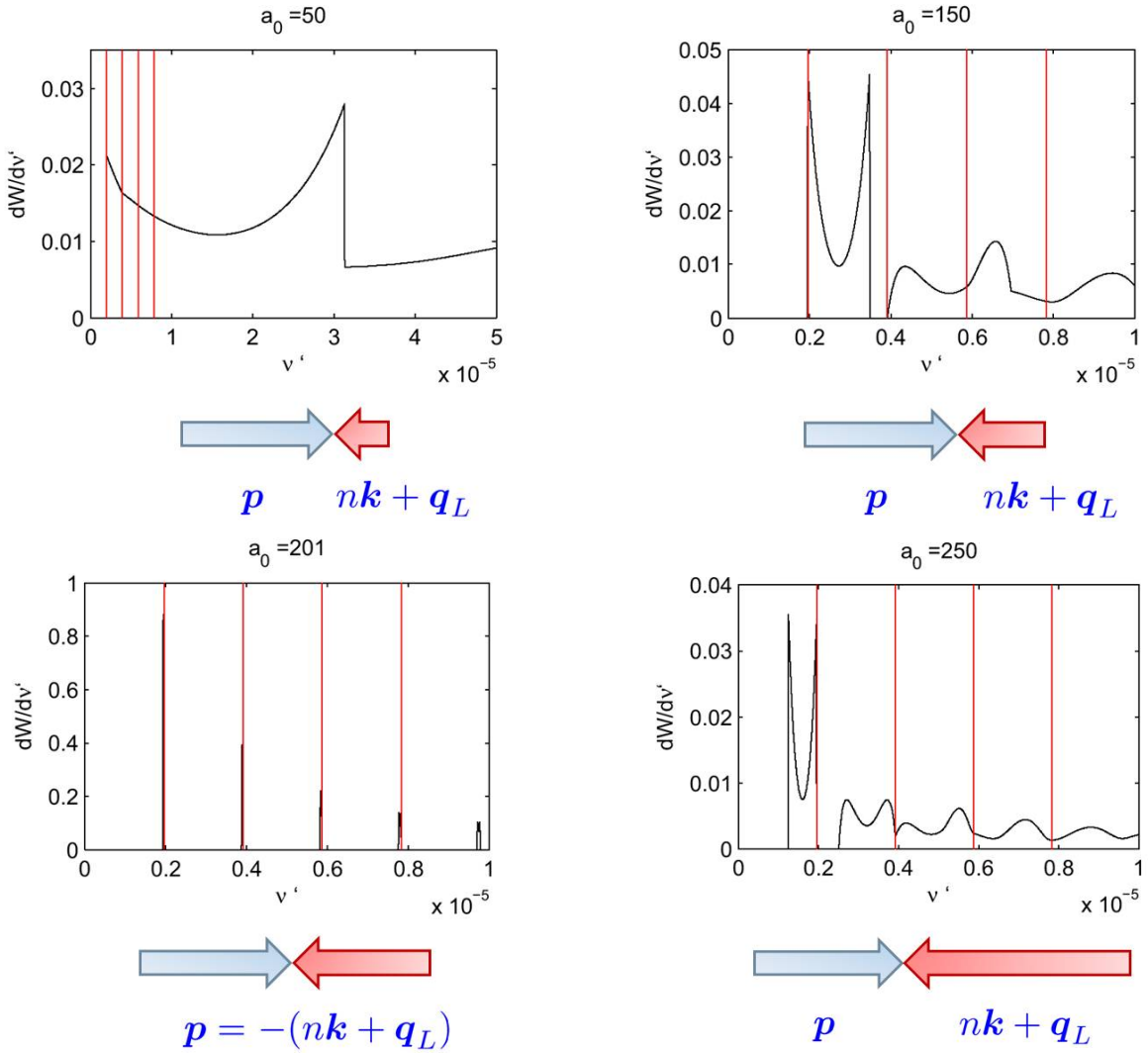

Figure 6. Illustration of the intensity dependent centre-of-mass frame where the total momentum changes direction (third panel). For inverse Compton scattering the electron momentum $\boldsymbol{p}$ dominates in magnitude implying a blue-shift of the scattered frequencies (upper panels). A red-shift results when $|n\boldsymbol{k} + \boldsymbol{q}_L| > |\boldsymbol{p}|$ (last panel).

The magnitude of the asymptotic electron momentum is fixed by the beam specifications, $|\boldsymbol{p}| = me^{\zeta}$. The laser contributes a momentum $n\boldsymbol{k} + \boldsymbol{q}_L$ along $\boldsymbol{k}$ to the total momentum, where $n\boldsymbol{k}$ is the laser momentum proper and the addition $\boldsymbol{q}_L$ changes $\boldsymbol{p}$ into the quasi-momentum $\boldsymbol{q}$, recall (4). This contribution grows linearly in magnitude with a_0, increasingly counterbalancing the incoming electron momentum $\boldsymbol{p}$ until exact compensation is achieved at $a_0 \simeq 2\gamma$. At this point the total momentum $\boldsymbol{P}$ changes direction, and the blue-shift turns into a red-shift.

4. Conclusion

We have given a short overview of the intensity signatures to be expected in the spectra of photons emitted in nonlinear Compton scattering. The main effects are: (i) a red-shift of the linear Compton edge implying a reduction in scattered frequency by a factor of approximately $1/a_0^2$, and (ii) the appearance of smaller side peaks corresponding to higher harmonics. The energy spectra evaluated in the lab frame depend quite sensitively on the value of a_0. Tuning a_0 from small to large values the individual harmonic spectra turn from being blue-shifted (inverse Compton scattering) to red-shifted. At the transition point, $a_0 \simeq 2\gamma$, the spectrum collapses to a line spectrum with peaks precisely at $\nu'_n = n\nu$.

Future work should address the use of more realistic beam shapes (in particular pulsed ones), processes related via crossing symmetry (pair creation and annihilation) and the influence of radiative corrections.

Acknowledgments

The author thanks Chris Harvey and Anton Ilderton for a fruitful collaboration and the organisers of the Workshop on Advanced QED Methods for Future Accelerators for their efforts resulting in such a stimulating environment.

References

[1] Bethe H and Heitler W 1934 *Proc. Roy. Soc. Lond.* **A146** 83–112
[2] Delbrück M 1933 *Z. Phys.* **84** 144
[3] The Vulcan 10 Petawatt Project: http://www.clf.rl.ac.uk/Facilities/vulcan/projects/10pw/10pw_index.htm
[4] The Extreme Light Infrastructure (ELI) project: http://www.extreme-light-infrastructure.eu
[5] Sauter F 1931 *Z. Phys.* **69** 742–764
[6] Coleman S R 1976 *Ann. Phys.* **101** 239
[7] Schwinger J S 1951 *Phys. Rev.* **82** 664–679
[8] Brezin E and Itzykson C 1970 *Phys. Rev.* **D2** 1191–1199
[9] Popov V S 1971 *Pisma Zh. Eksp. Teor. Fiz.* **13** 261–263 [JETP Lett. **13** 185 (1971)]
[10] Toll J 1952 PhD thesis, Princeton, 1952
[11] Narozhnyi N B 1968 *Zh. Eksp. Teor. Fiz.* **55** 714–721 [Sov. Phys. JETP **28**, 371 (1969)]
[12] Brezin E and Itzykson C 1971 *Phys. Rev.* **D3** 618–621
[13] Heinzl T *et al.* 2006 *Opt. Commun.* **267** 318–321 (*Preprint* `hep-ph/0601076`)
[14] Di Piazza A, Hatsagortsyan K Z and Keitel C H 2006 *Phys. Rev. Lett.* **97** 083603 (*Preprint* `hep-ph/0602039`)
[15] Harvey C, Heinzl T and Ilderton A 2009 *Phys. Rev.* **A79** 063407 (*Preprint* `0903.4151`)
[16] Bamber C *et al.* 1999 *Phys. Rev.* **D60** 092004
[17] Berestetskii V, Lifshitz E and Pitaevskii L 1982 *Quantum Electrodynamics (Course of Theoretical Physics, Vol. 4)* (Butterworth-Heinemann, Oxford)
[18] Heinzl T and Ilderton A 2009 *Opt. Commun.* **282** 1879–1883 (*Preprint* `0807.1841`)
[19] The HiPER project: http://www.hiper-laser.org/
[20] Jackson J 1999 *Classical Electrodynamics* (Wiley, New York) third edition
[21] Schott G 1912 *Electromagnetic Radiation* (Cambridge University Press)
[22] Landau L and Lifshitz E 1987 *The Classical Theory of Fields (Course of Theoretical Physics, Vol. 2)* (Butterworth-Heinemann, Oxford)
[23] Sengupta N 1949 *Bull. Math. Soc. (Calcutta)* **41** 187–198
[24] Sengupta N 1952 *Bull. Math. Soc. (Calcutta)* **44** 175–180
[25] Kibble T W B 1965 *Phys. Rev.* **138** B740–B753
[26] Volkov D 1935 *Z. Phys.* **94** 250–260
[27] Furry W H 1951 *Phys. Rev.* **81** 115–124
[28] Nikishov A I and Ritus V I 1963 *Zh. Eksp. Teor. Fiz.* **46** 776–796 [Sov. Phys. JETP **19**, 529 (1964)]
[29] Nikishov A I and Ritus V I 1964 *Zh. Eksp. Teor. Fiz.* **46** 1768–1781 [Sov. Phys. JETP **19**, 1191 (1964)]
[30] Narozhnyi N B, Nikishov A and Ritus V 1964 *Zh. Eksp. Teor. Fiz.* **47** 930 [Sov. Phys. JETP **20**, 622 (1965)]
[31] Bula C *et al.* 1996 *Phys. Rev. Lett.* **76** 3116–3119
[32] Chen S, Maksimchuk A and Umstadter D 1998 *Nature* **396** 653
[33] Babzien M *et al.* 2006 *Phys. Rev. Lett.* **96** 054802
[34] Compton A H 1923 *Phys. Rev.* **21** 483–502